Detection and Tracking of Underwater Pipes using a Magnetic Camera

Javier Garcia*, Ryan Lewis, Mohammadreza Shahsavar, Aaron T. Becker, and Julien Leclerc

Abstract—We present a magnetic camera system developed to detect ferrous or ferromagnetic objects. The main motivation is detection and tracking of underwater pipelines. Many industries, such as oil and gas, must perform inspection and maintenance of pipelines and automation is desirable. An electromagnet generates a static magnetic field which is read by an array of Hall-effect sensors. The presence of ferromagnetic materials distorts this field, which can be detected by the sensors and creates a magnetic image. The grid configuration of the camera allows for quick computation of the center of mass and general orientation of detected pipes, facilitating tracking. This camera is carried by an ROV and tested in a pool environment.

I. Introduction

Many tasks for underwater robotic agents include inspection and maintenance of underwater structures and assets. Unfortunately, sensing in deep sea environments is challenging. The darkness and turbidity greatly impact and even disable visual tracking and inspection, and only recently have those factors been studied to verify the robustness of vision-based systems [1]. The target may also be covered either by chance (sediment moving), or on purpose (buried pipelines).

Acoustic sensors are often employed for inspection, but they can be affected by environmental noise. Other methods such as ultrasound and radiography are difficult to perform if the pipe geometry is complex or its surface is not prepared for inspection. Since many underwater structures and assets are made out of metal, using electromagnetics is a reasonable approach. However, many electric methods require contact with the pipe, which is problematic if coatings are present. Magnetic methods do not require contact and have shown promise in detecting defects [2]. Underwater vehicles can carry said sensors to perform needed tasks [3], [4], [5].

This work analyzes the utility of using a Hall-effect sensor array for capturing images based on induced magnetic fields. The Hall-effect sensor array is mounted on the bottom of an aquatic remotely operated vehicle (ROV) along with a electromagnetic coil that is turned on in pulses. During each pulse, the Hall-effect sensor array takes a reading of the

This research is supported by Texas Commission on Environmental Quality through Subsea Systems Institute Award #582-21-10565. This project was paid for in part with federal funding from the Department of the Treasury through the State of Texas under the Resources and Ecosystems Sustainability, Tourist Opportunities, and Revived Economies of the Gulf Coast States Act of 2012 (RESTORE Act). The content, statements, findings, opinions, conclusions, and recommendations are those of the author(s) and do not necessarily reflect the views of the State of Texas or the Treasury. This work was also supported by the National Science Foundation under [1932572 2130793].

Authors are with the Department of Electrical and Computer Engineering, University of Houston, Houston, TX USA

*Corresponding author. Email:jgarciag@uh.edu



Fig. 1. (Left) Magnetic camera mounted underneath an ROV. (Right) ROV with camera hovering over an underwater ferrous pipe.

magnetic field, which is the sum of the field created by the coil and the field created by the magnetic response of the objects directly in front of each sensor. This measurement is then compiled into an image based on the magnitude of the response, which can be used for imaging and tracking ferrous pipelines. The grid configuration of the sensors facilitates calculation of the pipeline orientation. The current prototype can be seen in Figure 1.

II. RELATED WORK

A common way of performing metal detection is through inductive sensing [6]. A transmitting coil is excited, and the resulting signal in a receiving coil is measured. In the presence of ferromagnetic materials, the signal at the receiver will change. Underwater usage cases include detection of mines [7]. Unfortunately, inductance coupling is an undesirable effect that can be difficult to counteract [8]. The change in inductance necessitates an active method to keep the system in resonance. Using multiple coils also increases the weight that the ROV has to carry.

Instead of electromagnets, permanent magnets can be used to create the field. Systems following this approach have been implemented for detecting and guiding endoscopes [9], [10], [11], as well as medical robots [12], [13], [14]. Other works have developed ways to track passive magnets using Halleffect sensor arrays, such as [15] and the compliant device described in [16]. Magnetic fields have also been studied to inspect components inside home appliances [17]. Closer to our target application, [18] describes an array of magnets and magnetometers used to track ferromagnetic pipes in air.

While permanent magnets do not require excitation and thus save energy, we consider it useful to be able to control when the magnetic field is generated. This is important in situations when an external magnetic field affects other sensors, such as a compass. Strong permanent magnets also increase the risk of collision if the robotic agent has to maneuver very close to a ferromagnetic object, as it could become dangerously attracted to it.

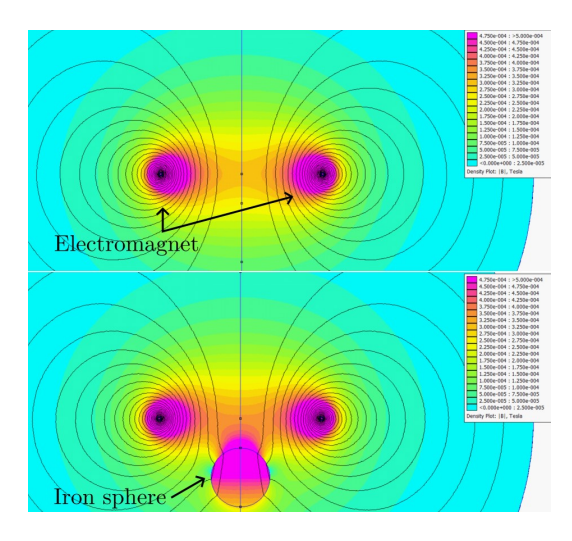


Fig. 2. 2D, axisymmetric, finite elements computation results showing the magnetic field produced by an electromagnet with and without a ferromagnetic sphere placed in proximity. The presence of an iron sphere distorts the field. The magnitude of the magnetic field is increased in the center of the electromagnet near the sphere. This simulation was performed using the software Finite Element Method Magnetics [21].

There is also much interest in detecting defects in pipes. Methods such as the one in [19] rely on inducing currents on the pipe. The resulting magnetic field is distorted by the defects, and the skin effect can be exploited to obtain more information [20]. The main drawbacks are the need to physically touch the pipe and to change frequency of excitation.

III. METHODS

A. Magnetic camera principle

In this paper we opted for using a DC magnetic pulse from a single coil, and an array of Hall-effect sensors located in the same plane as the coil. When ferromagnetic objects are near the energized coil, the generated magnetic field is distorted. A visual example is shown in Figure 2, where the intensity of the field has changed due the presence of an object.

The value of a magnetic field passing through an object with magnetization $\chi = \mu_r - 1$ is given by

$$B = \mu_0 (1 + \chi) H. \tag{1}$$

Above, H is the magnetic strength. A larger magnetization value results in a larger B field, which makes it easier to detect with a magnetometer.

Using an electromagnet, the strength of the magnetic field can be controlled to modify detection range. It also adds consistency by making the field perpendicular to the sensing elements, if they are located on the plane of the coil.

Our magnetic camera consists of a coil with N turns and an array of Hall-effect sensors with equal spacing. An instrumentation amplifier is used to focus on the range of measurements expected from the camera. To help choose the parameters of the amplifier, we performed several simulations with objects of different shapes and relative permeability values.

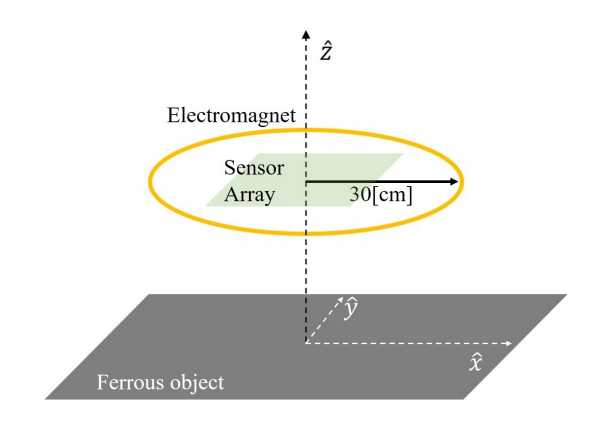


Fig. 3. Example setup of an Ansys simulation. The electromagnet is on the xy-plane and below it is a rectangular ferrous object (gray). The sensor array (green) is parallel to the plane of the electromagnet.

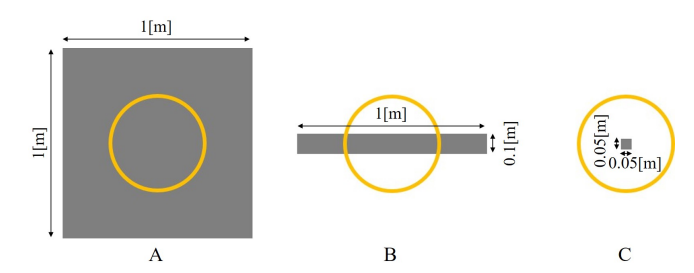


Fig. 4. Three ferrous objects were placed under the electromagnet in the Ansys simulations. (A) A large, 1[cm] thick plate, (B) a solid pipe, and (C) a small block.

B. Simulations of magnetic disturbance

Although equation (1) provides the mathematical basis to predict the presence of ferrous objects disturbing a magnetic field, in practice there are many relevant variables. Besides the composition of the object, its size, geometry, orientation, and distance from the magnetic camera will all affect the response. Many of those variables cannot be known beforehand.

Therefore, we limit this study to certain objects, like pipes, and limit the range of detection we are considering. This range is also limited by the signal-to-noise ratio (SNR) of our system. Furthermore, we are only interested in showing detection and tracking capabilities. Material classification is theoretically possible, but beyond the scope of this paper.

We took a simulation approach to better understand the response of the system to the ferrous objects and use the resulting data to help with the design of the magnetic camera hardware, as well as the controllers needed for the ROV carrying the camera. The software of choice is Ansys.

We modeled a coil with a radius of 30[cm] and 16 turns to serve as the electromagnet. The coil is on the xy-plane. A ferrous object is modeled at z=0, and the coil is moved along the z-axis. An example of a simulation setup is shown in Figure 3.

The responses to three different magnetic objects were simulated. These objects are a large metal plate, a long pipe, and a small cube. These can be seen in Figure 4. The large plate is $1[m] \times 1[m]$ with a 1[cm] thickness. The pipe is 1[m] long and has an outer diameter of 10[cm]. The small cube has side lengths of 5[cm]. The different geometries were chosen

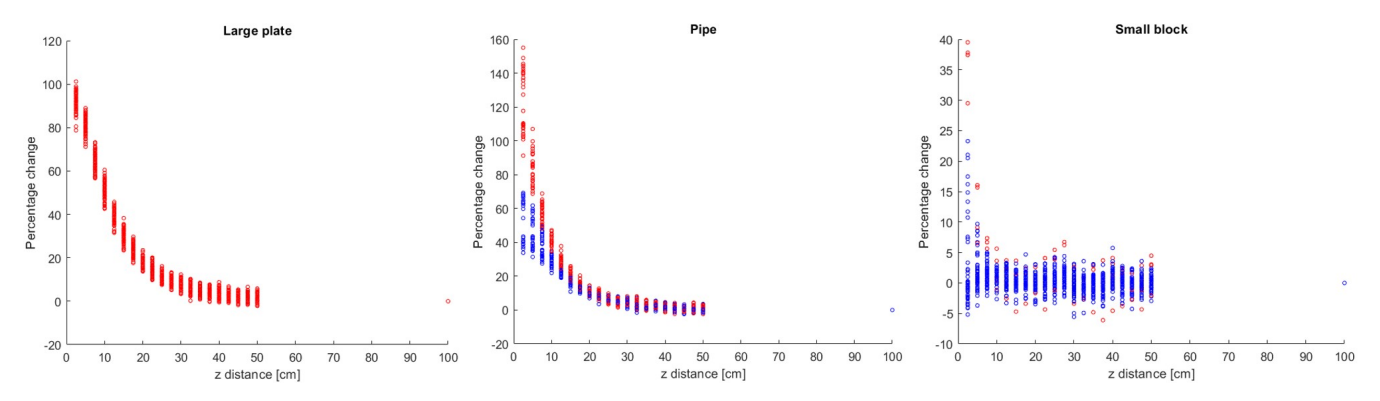


Fig. 5. The normalized data obtained for each object was compared to the reference point, at z = 100[cm]. These curves show the resulting percentage difference as the electromagnet gets closer to the object.

to study the effect of object overlap with the sensing array. The sensor array consists of 64 points, or pixels, arranged in a square configuration and centered on the coil. During the simulation, the coil is swept along the z-axis, starting from 50[cm] and moving in 2.5[cm] steps down to only 2.5[cm] away from the ferrous object. An extra simulation at z=100[cm] is performed as a reference point, which is the case when no object is expected to be detected.

Another important aspect is the decrease in current in the electromagnet as the system operates. This is because the most viable method for providing power to our electromagnet when mounted on our ROVs is a battery, which will drop in voltage as it sends pulses to the electromagnet. A workaround is to normalize the magnetic response with respect to the current. The simulations were performed with different currents flowing through the electromagnet, from 100[A] to 200[A] in 20[A] increments.

Next, the normalized data was compared to the reference point. The percentage change with respect to the reference is shown in Figure 5, for all three objects. The plots show the pixels right on top of the object as red dots, while blue dots indicate the rest of the pixels. An interesting effect is that at larger separations (around 10[cm]) the sensors on top of the pipe and the cube actually detect magnetic fields smaller than nominal. This is likely due to the demagnetization field, which arises when the field created by the electromagnet is concentrated by the ferrous objects, similar to a magnet [22].

C. Orientation of detected pipes

We also used Ansys and MATLAB to simulate the magnetic camera as it hovers over a ferrous pipe. This way we could test simple controllers for pipe tracking. The setup for this simulation consisted of the electromagnet moving in the xy-plane, as opposed to in the z-axis, with MATLAB requesting magnetic values at the pixel locations at every new location. A ferrous pipe was modeled 15[cm] under the camera.

The percentage change in the pixels was monitored. When the camera is positioned on top of the pipe, we expect the absolute percentage difference to increase for the pixels overlapping the pipe. The reference is the data taken at the beginning of the simulation, when the camera is far from the pipe. To track the pipe, it must be detected first and then its

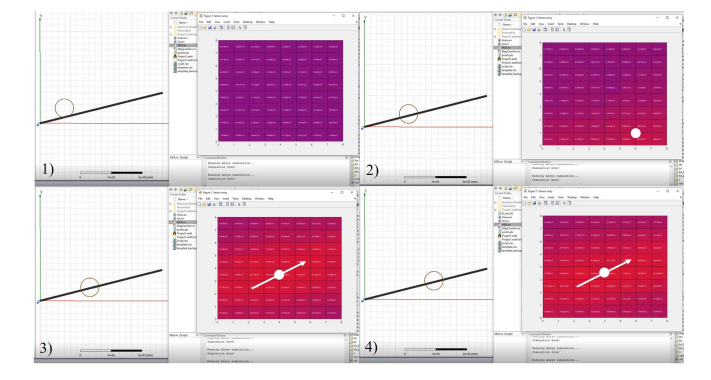


Fig. 6. Simulated pipe tracking. First, a reference snap is taken. Pixels are shown as dark purple when no ferrous objects are nearby. If several pixels turn red, the pipe has been detected. The robot then moves toward the pipe's center of mass, shown as a white dot. It follows the calculated orientation of the pipe (white line) for the rest of the simulation.

orientation calculated. For initial detection, we rely on the center of mass, which is given by

$$pipe_{com} = \frac{1}{\sum_{r,c} \mathcal{I}(r,c)} \left[\sum_{r,c} r \mathcal{I}(r,c), \sum_{r,c} c \mathcal{I}(r,c) \right],$$
 (2)

where r and c denote the row and column of the magnetic camera image, and $\mathcal{I}(r,c)$ is an indicator function evaluated at pixel r and c that is 1 if a pipe is detected and 0 otherwise. For the orientation calculation, we use the second moments of the image to calculate the angle as in [23]

$$pipe_{or} = atan2(2C_{1,1}, C_{2,0} - C_{0,2})/2$$
, where
$$C_{i,j} = \sum_{r,c} (r - pipe_{com,r})^i (c - pipe_{com,c})^j p(r,c).$$
(3)

If the calculated $pipe_{\rm com}$ is within a small margin of the camera's center, and the calculated $pipe_{\rm or}$ is aligned with the direction of travel, then we say that the camera is satisfactorily tracking the pipe. Thus, the basic process for a controller is to first detect the pipe, signaled by a minimum number of pixels showing a percentage change above a given threshold. Then, the camera is moved to center $pipe_{\rm com}$, after which the direction of travel is chosen to follow $pipe_{\rm or}$.

Figure 6 shows a sequence of frames demonstrating the tracking process. First, the electromagnet starts not hovering over the pipe to obtain the reference snap. Each next snap

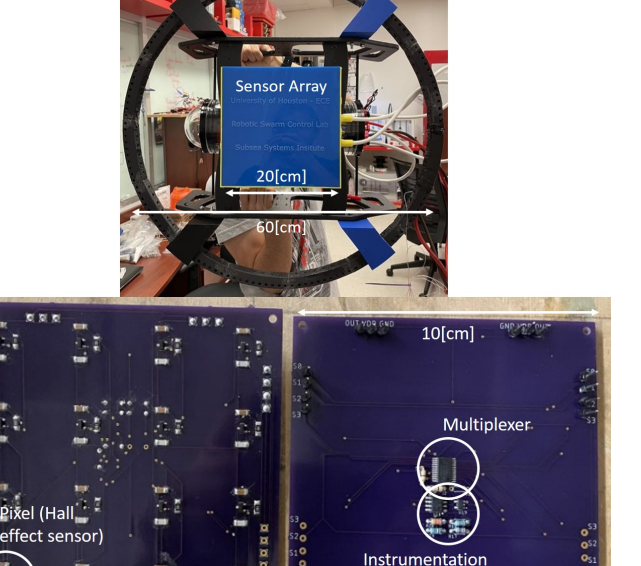


Fig. 7. Magnetic camera components. The sensor array is encased in silicone (blue). The electronics that control the camera are located in a watertight enclosure behind the array. Four custom PCBs are used.

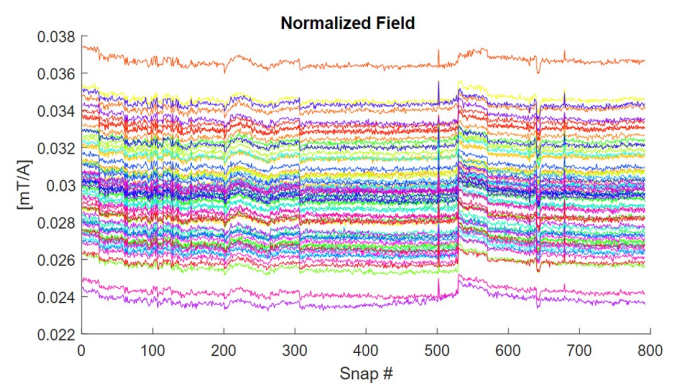


Fig. 8. Normalized values of all pixels for many continuous snaps. Ignoring some spiking, the values remained fairly constant.

is compared to the reference to calculate the percentage difference. When the difference is small, pixels are shown as dark purple. When the difference exceeds a threshold, the pixels are shown as red, and $pipe_{\rm com}$ is calculated. The robot is then moved to center the camera over the pipe, and then it is moved in the direction of $pipe_{\rm com}$. While tracking the pipe, small lateral adjustments can be made if $pipe_{\rm com}$ starts drifting away.

IV. TESTS AND RESULTS

A. Camera prototype

The camera prototype consists of a coil similar to the one used in the simulations. An 8×8 array of Hall-effect sensors are co-planar with the coil, and are spaced 2.5[cm] in both directions. This array is implemented by chaining four custom boards, each containing 16 sensors, a multiplexer to select the sensor output, and an instrumentation amplifier

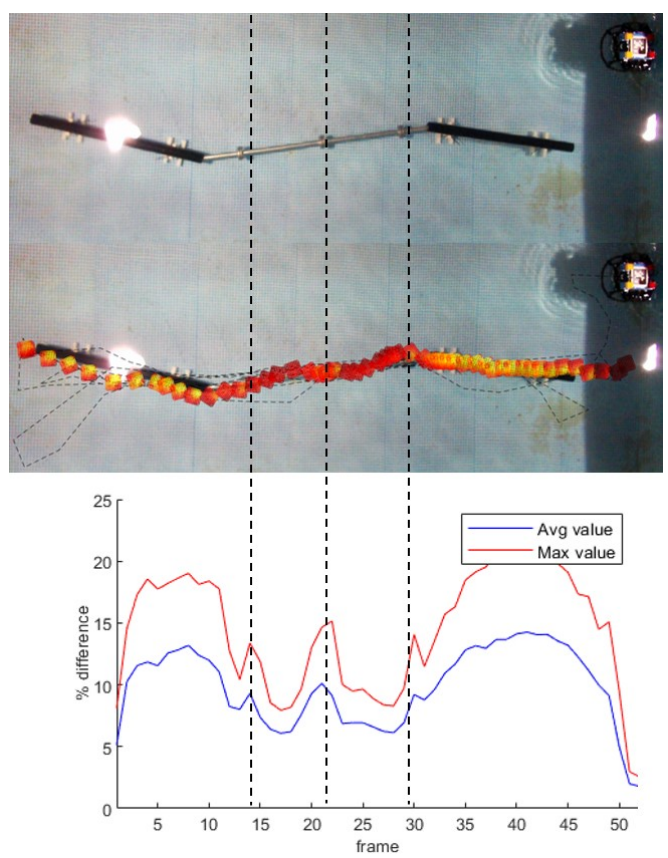


Fig. 9. Magnetic camera's pixel values as a pipeline is scanned. The change in diameter, as well as the flanges of the thinner pipe, can be observed.

(Figure 7). Using a multiplexer was a design choice that enables further scalability, but has the downside of requiring more time to sample all sensors.

The Hall-effect sensor chosen is the DRV2023EA, which is bipolar, analog, and has a range of -18[mT] to 18[mT]. We designed our camera to work with 180[A] pulses, so the instrumentation amplifier parameters were chosen to maximize sensitivity around that point. Figure 8 shows the magnetic field measured by the sensors, without any ferrous objects present, normalized by the electromagnet current as the power supply depletes.

B. Pipeline mapping

The prototype was tested in a pool environment about 1.5[m] deep. Ferrous pipes were placed in the pool, and the ROV was manually driven over the pipes. An overhead camera was used to obtain the true pose of the ROV. The distance between the pipes and the camera was around 20[cm]. Every two seconds, MATLAB acquired a magnetic camera snap and an overhead camera snap. Figure 9 shows a pipe with three segments being mapped. The black segments are 12[cm] in diameter and with wall thickness of 6[mm], and the middle one is 6[cm] diameter with 4[mm] wall thickness. The middle segment also contains three flanges, (15[cm] diameter), which our camera can detect due to the resulting stronger magnetic disturbance (brighter spots).

The pipe orientation calculation based on the camera's readings was also tested in post-processing. Using (3), the

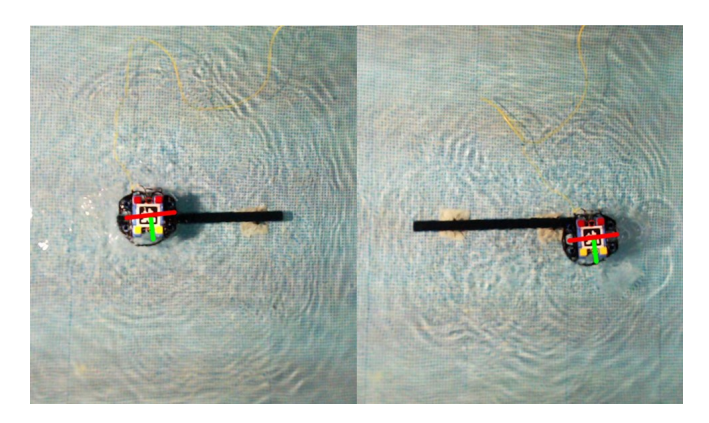


Fig. 10. Calculated pipe orientation (red) in two different instances of the ROV hovering over a pipe. The pose and orientation of the ROV (green) are calculated using the overhead camera's footage.

orientation was drawn as a red line on the overhead picture, with a green line showing the orientation of the ROV, as shown in Figure 10. Even though there is a slight delay between the magnetic camera and overhead camera snaps, the calculated orientations match the pipe enough to use for automatic control.

C. Pipeline tracking

We implemented a simple algorithm to test the pipe tracking capabilities of our system. First, the ROV moves forward until the camera detects an object (pipe). Once the pipe has been detected, the ROV centers with the center of mass of the object (2), then it turns in a predetermined direction until

its forward axis is aligned with the calculated orientation (3). The ROV then follows the pipe while correcting orientation and lateral errors.

The performance of the tracking was quantified by computing the distance between the centroid of the ROV and the closest point on the pipeline for every frame. The orientation error between the ROV's forward axis and the pipeline at the same point was also computed. The overhead camera was used only for this analysis, with the magnetic camera data being the only feedback for the ROV control. Several runs where performed, and Figure 11 shows the tracking performance for three pipelines with different characteristics. The start and end frames of the actual tracking are indicated, as well as the zero orientation error lines. The magnetic activity, in terms of the percentage difference seen by the camera during the run, is also shown.

The ROV manages to closely track the pipelines, with the distance error staying below 25[cm] for the most part. The sensor array covers enough area to keep the pipeline in sight and rectify the error. However, considerable oscillation takes place while tracking. The main reason is that the magnetic camera takes a snap every two seconds to conserve battery life and to prevent overheating of the components that control power flow to the electromagnet. After calculating the control effort, the ROV is moved accordingly in an open-loop fashion until the next snap. Further limiting the thrust outputs of the ROV to avoid overshoot was not possible due to the inertia of the system.

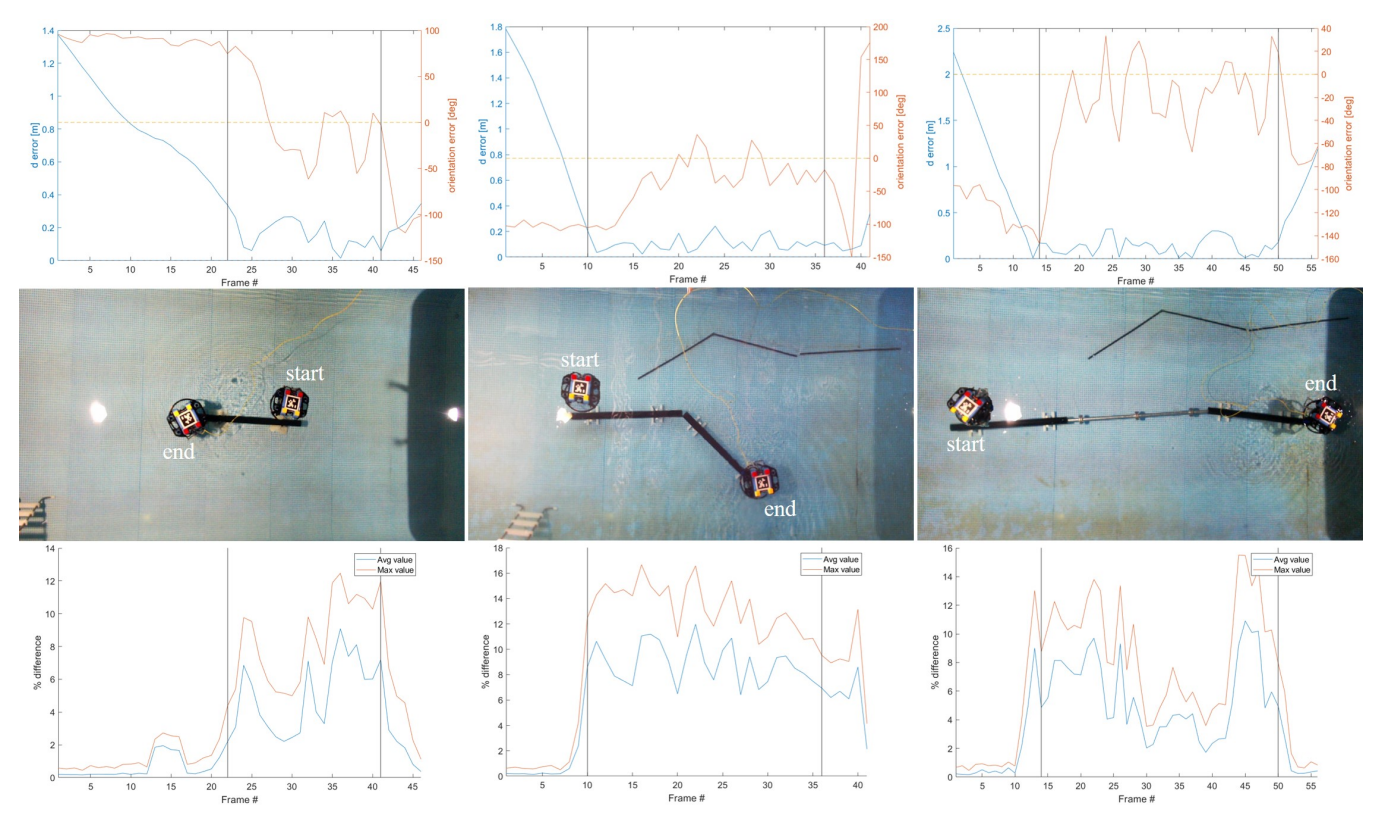


Fig. 11. Analysis of tracking performance for three different pipelines. The vertical black lines indicate when the tracking actually starts. The top plots show the distance between the center of the ROV and the closest point on the pipeline, as well as the respective orientation error. The bottom plots show the maximum and average percentage difference measured by the magnetic camera.

V. CONCLUSION

In this paper we presented a magnetic camera consisting of an electromagnet and a 2D array of Hall-effect sensors. This camera was used to provide an ROV with information about surrounding ferrous objects underwater.

The magnetic camera was designed based on simulation results, mounted on the ROV and then tested in a pool. It allowed the ROV to map underwater ferrous pipes and detect some geometric features, such as changes in diameter and flanges. The ROV was also able to find pipelines and track them, relying entirely on the feedback from the magnetic camera.

For future work we will test different sensors. While the Hall-effect sensors are straightforward to use, tunnel magnetoresistance sensors are promising in terms of better SNR and sensitivity. We are also interested in different array configurations, such as a denser single row of sensors for mapping. While the magnetic camera can detect some pipeline features, we are working on being able to extract even more information such as material composition and corrosion/presence of defects. Permanent magnets also offer advantages such as much lower power usage and higher data acquisition rates.

The controller for the pipe tracking can also be improved by increasing the magnetic feedback rate and implementing a predictive controller. In addition, we want to incorporate multiple magnetic cameras on the same ROV so that we can perform 3D collision avoidance.

REFERENCES

- [1] M. Myint, K. N. Lwin, N. Mukada, D. Yamada, T. Matsuno, Y. Toda, S. Kazuhiro, and M. Minami, "Experimental verification of turbidity tolerance of stereo-vision-based 3d pose estimation system," *Journal* of marine science and technology, vol. 24, no. 3, pp. 756–779, 2019.
- [2] M. Ho, S. El-Borgi, D. Patil, and G. Song, "Inspection and monitoring systems subsea pipelines: A review paper," *Structural Health Monitoring*, vol. 19, no. 2, pp. 606–645, 2020.
- [3] L. Li, R. Zhang, W. Liu, Z. Li, and L. Li, "Magnetic signature measurement of surface ship using a ROV-equipped with magnetometer," in *Global Oceans* 2020: Singapore U.S. Gulf Coast. IEEE, 2020, pp. 1–5.
- [4] S. Scudero, G. Vitale, A. Pisciotta, R. Martorana, P. Capizzi, and A. D'Alessandro, "Remotely controlled aerial and underwater vehicles in support to magnetic surveys," *International Conference on Metrol*ogy for Archaeology and Cultural Heritage, 2019.
- [5] C. Rühlemann, U. Barckhausen, S. Ladage, L. Reinhardt, and M. Wiedicke, "Exploration for polymetallic nodules in the German license area." ISOPE, 2009.
- [6] H. Ewald and H. Krüger, "Inductive sensors and their application in metal detection," in *International Conference on Sensing Technology*, New Zealand, 2005.
- [7] L. Riggs, S. Chilaka, L. Collins, L. Lowe, and R. Weaver, "Discrimination experiments with the U.S. Army's standard metal detector," *Radio science*, vol. 39, no. 4, pp. RS4S06–n/a, 2004.
- [8] D. Ambruš, D. Vasić, and V. Bilas, "Active induction balance method for metal detector sensing head utilizing transmitter-bucking and dual current source," *Journal of physics. Conference series*, vol. 450, no. 1, 2013.
- [9] M.-C. Kim, E.-S. Kim, J.-O. Park, E. Choi, and C.-S. Kim, "Robotic localization based on planar cable robot and Hall sensor array applied to magnetic capsule endoscope," *Sensors (Basel, Switzerland)*, vol. 20, no. 20, pp. 5728–5746, 2020.
- [10] M. Wang, S. Song, J. Liu, and M. Q.-H. Meng, "Multipoint simultaneous tracking of wireless capsule endoscope using magnetic sensor array," *IEEE transactions on instrumentation and measurement*, vol. 70, pp. 1–10, 2021.

- [11] Q. Zhang, Y. Li, H. Xu, X. Li, and X. Zhang, "Magnetic localization method of capsule endoscope based on hybrid model," *IEEE transactions on instrumentation and measurement*, vol. 72, pp. 1–10, 2023.
- [12] D. Son, S. Yim, and M. Sitti, "A 5-D localization method for a magnetically manipulated untethered robot using a 2-D array of Halleffect sensors," *IEEE/ASME transactions on mechatronics*, vol. 21, no. 2, pp. 708–716, 2016.
- [13] K. Li, Y. Xu, Z. Zhao, and M. Q.-H. Meng, "External and internal sensor fusion based localization strategy for 6-DOF pose estimation of a magnetic capsule robot," *IEEE robotics and automation letters*, vol. 7, no. 3, pp. 6878–6885, 2022.
- [14] M. Zhang, L. Yang, C. Zhang, Z. Yang, and L. Zhang, "Simultaneous actuation and localization of magnetic robots using mobile coils and eye-in-hand Hall-effect sensors," in 2021 IEEE/RSJ International Conference on Intelligent Robots and Systems (IROS). IEEE, 2021, pp. 8515–8521.
- [15] V. Schlageter, P.-A. Besse, R. Popovic, and P. Kucera, "Tracking system with five degrees of freedom using a 2D-array of Hall sensors and a permanent magnet," *Sensors and actuators. A, Physical*, vol. 92, no. 1, pp. 37–42, 2001.
- [16] N. Fischer, J. Kriechbaum, D. Berwanger, and F. Mathis-Ullrich, "Compliant Hall-effect sensor array for passive magnetic instrument tracking," *IEEE sensors letters*, vol. 7, no. 3, pp. 1–4, 2023.
- [17] B. A. Tuan, A. de Souza-Daw, H. M. Phuong, T. M. Hoang, and N. T. Dzung, "Magnetic camera for visualizing magnetic fields of home appliances," in 2014 IEEE Fifth International Conference on Communications and Electronics (ICCE), 2014, pp. 370–375.
- [18] X. Huang, Y. Wang, J. Ma, J. Wu, J. Li, Y. Zhang, and H. Feng, "A localization method for subsea pipeline based on active magnetization," *Measurement science and technology*, vol. 34, no. 2, 2023.
- [19] R. Jarvis, P. Cawley, and P. Nagy, "Current deflection NDE for the inspection and monitoring of pipes," NDT and E international: independent nondestructive testing and evaluation, vol. 81, pp. 46– 59, 2016.
- [20] A. Sophian, G. Tian, D. Taylor, and J. Rudlin, "Electromagnetic and eddy current NDT: a review," *Insight*, vol. 43, no. 5, pp. 302–306, 2001.
- [21] D. Meeker, "Finite element method magnetics," https://www.femm. info/.
- [22] G. M. Wysin, "Demagnetization fields," https://www.phys.ksu.edu/ personal/wysin/notes/demag.pdf, 2012.
- [23] M. W. Spong, S. Hutchinson, and M. Vidyasagar, Robot modeling and control. John Wiley & Sons, 2020.